Carbon Dioxide Separation and Dry Reforming of Methane for Synthesis of Syngas by a Dual-phase Membrane Reactor

Matthew Anderson and Y.S. Lin
School for Engineering of Matter, Transport and Energy, Arizona State University, Tempe, AZ 85287-6106

DOI 10.1002/aic.14103
Published online April 8, 2013 in Wiley Online Library (wileyonlinelibrary.com)

High-temperature CO_2 selective membranes offer potential for use to separate flue gas and produce a warm, pure CO_2 stream as a chemical feedstock. The coupling of separation of CO_2 by a ceramic–carbonate dual-phase membrane with dry reforming of CH_4 to produce syngas is reported. CO_2 permeation and the dry reforming reaction performance of the membrane reactor were experimentally studied with a CO_2–N_2 mixture as the feed and CH_4 as the sweep gas passing through either an empty permeation chamber or one that was packed with a solid catalyst. CO_2 permeation flux through the membrane matches the rate of dry reforming of methane using a 10% Ni/γ-alumina catalyst at temperatures above 750°C. At 850°C under the reaction conditions, the membrane reactor gives a CO_2 permeation flux of 0.17 mL min^{-1} cm^{-2}, hydrogen production rate of 0.3 mL min^{-1} cm^{-2} with a H_2 to CO formation ratio of about 1, and conversion of CO_2 and CH_4, respectively, of 88.5 and 8.1%. © 2013 American Institute of Chemical Engineers *AIChE J*, 59: 2207–2218, 2013
Keywords: carbon dioxide separation, molten carbonate, syngas production, hydrogen production, membrane reactor

Introduction

A great need has been placed on the ability to separate and sequester CO_2, especially as the debate over global warming rages on. The primary source of CO_2 emissions is flue gas from coal-fired electrical power plants. CO_2 captured from flue gas can be sequestered by various methods, such as underground injection or storage as mineral carbonates (i.e., $CaCO_3$). Alternatively, streams of warm, highly concentrated CO_2 can also be used as a feedstock for chemical synthesis of syngas. Syngas, a mixture of hydrogen (H_2) and carbon monoxide (CO), can be used to make a number of important chemical products including ethylene, ethylene glycol, various alcohols and diesel fuel.[1] It can also be used in the manufacture of ammonia-based products for fertilizer production[2] and in the Fischer–Tropsch process to synthesize liquid fuels.[3–5] Production of syngas can be accomplished via a number of different reaction pathways which are discussed as follows.

Steam reforming of methane (CH_4) is the process that is almost exclusively used to produce syngas commercially at the present moment.[2] Here, CH_4 reacts with water vapor to form the H_2/CO gas mixture, as shown

$$CH_4 + H_2O(v) \leftrightarrow CO + 3H_2 \quad \text{(A)}$$

There are several negative aspects for using Reaction A for syngas production. First, the reaction is endothermic ($\Delta H^0_{298} = 206$ kJ mol^{-1}) and must be carried out at high temperature, thus requiring substantial energy and capital investment to sustain a high throughput process.[6–8] Furthermore, the H_2:CO ratio produced in the reaction is 3:1. Synthesis of many fuels, especially those via the Fischer–Tropsch process, are more efficient if the H_2:CO ratio is as close to 1 as possible.[8,9] Lastly, the failure to remove sulfur containing compounds in the methane stream can poison the catalysts in the packed bed and lead to lower reaction conversions over time.

Another method that can be used to produce syngas is by the direct partial oxidation of methane. Here, methane reacts with O_2 to form the syngas mixture as shown

$$CH_4 + {}^1/_2O_2 \leftrightarrow CO + 2H_2 \quad \text{(B)}$$

Direct partial oxidation is mildly exothermic ($\Delta H^0_{298} = -36$ kJ mol^{-1}) and produces H_2 and CO in a ratio of 2:1. Although the H_2:CO ratio is closer to the desired figure for methanol and Fischer–Tropsch fuel synthesis, the reaction scheme is not without drawbacks. The major disadvantage centers on the reactivity of H_2 and CO with oxygen. Both products can be further oxidized to produce CO_2 and H_2O. Therefore, this particular method is only suitable for reactors with extremely short residence times.[6,7,10,11] Additionally, due to the formation of CO_2 and H_2O during the direct partial oxidation reaction, it is thought that the actual mechanism of syngas production occurs via the exothermic combustion reaction ($\Delta H^0_{298} = -802$ kJ mol^{-1})

$$CH_4 + O_2 \leftrightarrow CO_2 + 2H_2O \quad \text{(C)}$$

and the endothermic dry reforming reaction ($\Delta H^0_{298} = 247$ kJ mol^{-1})

$$CH_4 + CO_2 \leftrightarrow 2CO + 2H_2 \quad \text{(D)}$$

Correspondence concerning this article should be addressed to Y. S. Lin at jerry.lin@asu.edu

© 2013 American Institute of Chemical Engineers

A major drawback of Reaction C is that it requires a feed stream of pure oxygen into the system.[7,9] For this reason, a cryogenic oxygen plant would be required. This would increase costs dramatically.[12] Moreover, this particular process would have to be designed to avoid against the occurrence of hot spots and potential reactor runaway, as Reaction C is very exothermic.

The dry reforming reaction shown in Reaction D produces synthesis gas at a H_2:CO ratio of 1:1 which is highly suitable for liquid fuel synthesis. Using this reaction to produce syngas would eliminate the need for a feed stream of pure oxygen and all of the shortcomings that accompany Reaction C. In addition, unlike Reactions A–C, the dry reforming reaction uses two greenhouse gases, CO_2 and CH_4, to create a valuable chemical feedstock.[13] Several potential side reactions accompany the dry reforming reaction, including the reverse water gas shift reaction,[14] the methane cracking reaction[15] and the Boudouard reaction.[16] Another downside is the fact that catalysts used are prone to carbon deposition from the methane cracking and Boudouard reactions as a result of the lower H to C ratio.[17] Yet, despite these undesirable characteristics, Reaction D remains a viable method for syngas production.

The standard Gibbs free energy change for the endothermic Reaction D decreases with increasing temperature and becomes zero at a temperature of about 917 K (644°C).[12] Therefore, to achieve high conversion, the operating temperatures for dry reforming of methane should be above 644°C. Several groups have studied the use of hydrogen-selective membrane reactors to enhance the production of syngas via the dry reforming reaction by removing H_2. Oyama and coworkers[1,18] compared the dry reforming of methane in a simple plug flow reactor and in another that contained a hydrogen selective membrane. The addition of a Vycor glass membrane to the reactor resulted in methane conversions above thermodynamic equilibrium. Gallucci et al.[19] used porous tubular palladium–silver membranes selective to H_2 in conjunction with an alumina supported Ni catalyst for dry reforming of methane. The porous membranes were found to offer higher CO_2 and CH_4 conversions of 20.6 and 17.41%, compared to 14.0 and 8.4% without a membrane. Bosko et al.[20] performed the dry reforming reaction in membrane reactors using a Pd and Ad-Ag composite and achieved a methane conversion of 80% at 450°C.

Recently, Anderson and Lin[21] demonstrated that a dual-phase ceramic–carbonate membrane consisting of a $La_{0.6}Sr_{0.4}Co_{0.8}Fe_{0.2}O_{3-\delta}$ (LSCF) support infiltrated with a 42.5/32.5/25 mol % $Li_2CO_3/Na_2CO_3/K_2CO_3$ molten carbonate mixture was capable of separating CO_2 from CO_2 containing gas mixture at high temperature. The membrane separates CO_2 based on the mechanism with the following forward reaction occurring on the upstream (feed side) membrane surface

$$CO_2 + O^{=} \leftrightarrow CO_3^{=} \qquad \text{(E)}$$

where oxygen ions ($O^{=}$) from the support are transferred from the other side of membrane, as shown in Figure 1. Carbonate ions formed on the upstream membrane surface transport through the carbonate phase of the membrane. On the downstream (sweep side) membrane surface, the reverse of Reaction E occurs, releasing carbon dioxide and oxygen ions which transport back through the ceramic phase to the upstream membrane surface. CO_2 flux through the LSCF dual-phase membrane varied from 0.039 to 0.282 mL min^{-1} cm^{-2} from 700–900°C for a 1.5-mm-thick membrane.[21]

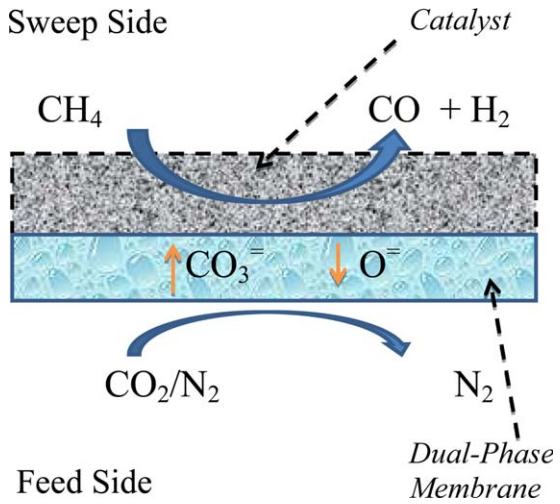

Figure 1. Schematic illustration of membrane reactor with a carbon dioxide perm-selective ceramic–carbonate dual-phase membrane coupling carbon dioxide separation with dry reforming of methane.

[Color figure can be viewed in the online issue, which is available at wileyonlinelibrary.com]

The operating temperature for the dual-phase membrane appears to match the reaction temperature for the dry reforming of methane (> 700°C). Thus, the membrane offers potential for use directly in a membrane reactor packed with an adequate catalyst for carbon dioxide separation and dry reforming of methane, as illustrated in Figure 1. A CO_2 containing mixture (such as flue gas) is fed to one side of the membrane and methane to the other packed with a catalyst. CO_2 permeates through the membrane and reacts with methane on the downstream side. The membrane reactor achieves CO_2 separation and dry reforming reaction using a single device—a membrane reactor system. This article reports on an experimental study of the use of the ceramic–carbonate dual-phase membrane as a membrane reactor in conjunction with the dry reforming reaction for carbon dioxide capture and synthesis of syngas. Another objective of this article is to study carbon dioxide permeation through the ceramic–carbonate dual-phase membrane with the occurrence of a reaction on the downstream side.

Experimental

Synthesis of the $La_{0.6}Sr_{0.4}Co_{0.8}Fe_{0.2}O_{3-\delta}$–carbonate dual-phase membranes

$La_{0.6}Sr_{0.4}Co_{0.8}Fe_{0.2}O_{3-\delta}$ (LSCF) powder was synthesized via the liquid citrate method according to the procedure described by Anderson and Lin.[21] To form supports of 1.5 mm in thickness, 3.0 g of the LSCF powder and PVA binder mixture was placed into a 30 mm stainless steel mold and pressed to 160 MPa for 5 min in a Carver hydraulic press. The green disks were sintered in air for 24 h at 900°C (2°C min^{-1} ramp rate) to produce mechanically stable, porous supports of about 20 mm in diameter and 1.5 mm in thickness, with the appropriate pore size. The porous supports were infiltrated with the 42.5/32.5/25 mol % $Li_2CO_3/Na_2CO_3/K_2CO_3$ molten carbonate mixture to obtain dense dual-phase membranes via the direct infiltration method.[21,22]

Synthesis of the $La_{0.6}Sr_{0.4}Co_{0.8}Fe_{0.2}O_{3-\delta}$ and 10% Ni/γ-alumina catalysts

The same composition of powder $La_{0.6}Sr_{0.4}Co_{0.8}Fe_{0.2}O_{3-\delta}$ (LSCF) used to prepare the supports for the dual-phase membrane was used for the LSCF combustion catalyst. As such, the same method was used to make catalyst.[21] After calcination at 600°C, the powder was reground with a mortar and pestle and then sintered for 24 h at 900°C (ramp rate of 2°C min^{-1}). To further decrease the particle size, the powder was placed into a Teflon tumbler and mixed with ethanol. The tumbler was filled with three parts ethanol to one part powder by weight to form a slurry. Zirconia balls of 2 and 5 mm in diameter were added to the tumbler and the resulting slurry was ball milled for 48 h. After ball milling, the ethanol was evaporated from the slurry and the remnants were reground for use as the catalyst in the dry reforming experiments.

To synthesize the 10 wt % Ni/γ-alumina reforming catalyst, appropriate amounts of $Ni(NO_3)_2{\cdot}6H_2O$ (Alfa Aesar, 98%) and γ-alumina (Alfa Aesar) were obtained. Pellets of γ-alumina were ground with a mortar and pestle and then separated with a #80 sieve. Sieving was done to assure that all of the particles used for the catalyst were less than 180 μm in size. The $Ni(NO_3)_2{\cdot}6H_2O$ and sieved γ-alumina were mixed with deionized water at room temperature. The solution was then heated to 80°C and mixed thoroughly to allow for Ni to coat the γ-alumina particles. The temperature of the slurry was raised to 120°C and left overnight to allow all of the water to evaporate. The remnants were ground with a mortar and pestle and then calcined for 4 h at 700°C (ramp rate of 5°C min^{-1}). The calcined material was then reduced in a 10% H_2/He gas mixture for 6 h at 600°C to activate the catalyst. This step was performed twice.

All catalysts and membranes were characterized by X-ray diffraction in the 2θ range of 20° to 80° with a step size of 0.05°/s (Bruker D8, Cu Kα radiation). The supports and infiltrated membranes were characterized by room-temperature helium permeation measurements. Nitrogen porosimetry experiments on both catalysts were carried out at liquid nitrogen temperature (77K) using a Micromeretics ASAP 2020 to determine the average pore size and surface areas.

High-temperature CO_2 separation and reaction in membrane reactor

High-temperature CO_2 flux measurements were conducted using a similar high-temperature setup to the one described in previous work.[21] A schematic of the setup is shown in Figure 2 to illustrate placement of the catalyst within the system. A dual-phase membrane disk was sealed to the inner alumina tube (2.54 cm OD) by creating a paste composed of a mixture of ground, sintered LSCF powder (40 wt%), ground Pyrex™ beaker glass (50%), sodium aluminum oxide (Alumina·Na_2O; 10%) and water.[23] A 2.50 cm OD stainless steel ring was placed on top of the membrane. Appropriate amounts of LSCF (1.0 g) and Ni/γ-alumina (0.6 g) catalyst were added into the ring to form a consistent bed height of 3 mm.

The catalyst and membrane system were sealed inside a 3.8 cm OD alumina tube and heated at a rate of 1°C min^{-1} to 850°C to allow for the seal to soften and set. Gases were delivered to the up and downstream sides of the membrane by connecting mass flow controllers to 1 cm OD alumina tubes. Each tube was placed about 3 cm away from the membrane on both sides. The composition (25% CO_2, 75% N_2) and flow rate (100 mL min^{-1}) of the feed stream were kept constant throughout this entire study. Methane composition and flow

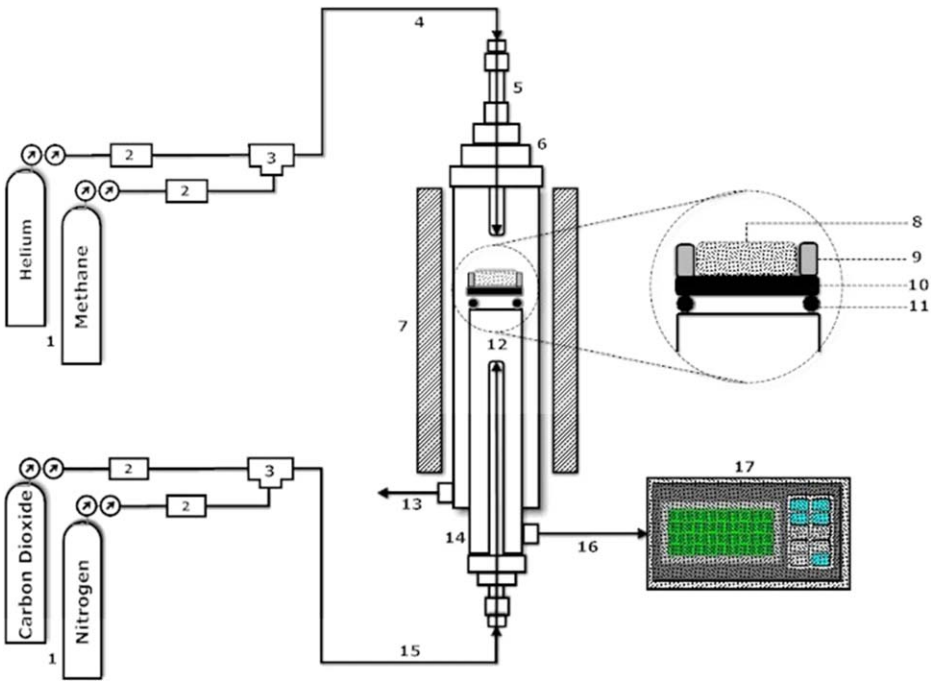

Figure 2. Schematic of high-temperature CO_2 permeation and reaction set up used in this work.

1) Gas cylinders, 2) Mass flow controllers, 3) Gas mixing tees, 4) Methane feed line, 5) Sweep gas (methane) tube, 6) Outer tube, 7) Furnace, 8) Catalyst, 9) Stainless steel ring, 10) Dual-phase membrane, 11) Ceramic seal, 12) Feed gas (CO_2), 13) Effluent for sweep gas, 14) Inner tube, 15) feed gas (CO_2) tube, 16) Effluent for feed gas, 17) Gas chromatograph. [Color figure can be viewed in the online issue, which is available at wileyonlinelibrary.com]

Table 1. Summary of Experimental Variables and Constants in Dry Reforming Experiments

Experiment Set	Variable	Constants	
1	Methane percentage (10–50%)	Sweep rate (10 mL·min^{-1})	Temperature (850°C)
2	Sweep rate (10–50 mL·min^{-1})	Methane percentage (50%)	Temperature (850°C)
3	Temperature (750–850°C)	Methane percentage (50%)	Sweep rate (10 mL min^{-1})

rate of the downstream (sweep) gases were varied based on the experiment conducted (see Table 1). For each of the scheduled experiments, the permeate and retentate flow rates were measured using a bubble flow meter, while the gas composition was determined by a gas chromatographer (Agilent, 6890N) with a packed column (2836PC, Alltech) and a TCD detector. Error associated with permeation measurements was found to be within ±5.6%. Errors associated with flux, conversion, and H_2 production calculations were slightly higher (roughly in the 8% range) due to difficulty in measuring the permeation area of the membrane placed in the high-temperature reactor.

Results and Discussion

General properties of the LSCF–carbonate dual-phase membrane and catalysts

Prior to using the LSCF dual-phase membrane for CO_2 separation and as a membrane reactor for the dry reforming reaction, the support and infiltrated membranes were characterized. The LSCF supports (not infiltrated with the carbonate) had a room-temperature helium permeance on the order of 10^{-6} mol m^{-2} s^{-1} Pa^{-1}. The supports had an average pore diameter of 365 nm, which was measured by a helium permeation method, and confirmed by mercury porosimetry and SEM. After infiltration with the carbonate, the room-temperature helium permeance of the dual-phase membrane decreased by four orders of magnitude to 10^{-10} mol m^{-2} s^{-1} Pa^{-1}, approaching the measuring capability limit of the permeation setup. Complete infiltration of the support was also confirmed via SEM imaging.[21] The drastic drop in helium permeance between the support and dual-phase membrane indicated that molten carbonate completely infiltrated the tortuous pores via capillary action to form a dense membrane. This is a stringent requirement toward producing a CO_2 selective membrane at high temperature, as formation of a gas tight dual-phase membrane ensures that only CO_2 will permeate through the membrane at high temperatures.

XRD patterns of the LSCF support and infiltrated membrane are shown in Figure 3. The pattern of the sintered support confirms that LSCF was properly synthesized via the citrate method, as the peaks and indices match that which has been reported previously by Wang et al.[24] Supports synthesized in this manner are of the desired perovskite structure and possess the characteristics essential for the dual-phase membrane. The XRD pattern of the noncontact side of the membrane after infiltration shows peaks indicative of molten carbonate at 2θ values of 21.9, 29.4, and 37.3° in Figure 3. The presence of the molten carbonate peaks on the noncontact side confirms complete infiltration throughout the entire thickness of the membrane.

Three different membrane reactor systems for syngas synthesis by dry reforming of CO_2 and CH_4 were studied. The first system dealt with a membrane reactor that contained no catalyst on the downstream side. This configuration was conceived to determine whether or not the surface of the dual-phase membrane could serve as a vehicle to drive the dry reforming reaction. For the two other arrangements, catalysts were packed on the downstream side of the membrane, as previously described and illustrated in Figures 1 and 2.

Some studies point toward the effectiveness of perovskite powders as catalysts for use in reactions involving the conversion of methane to syngas.[25,26] Toward this, the first type of catalyst studied in this work was a LSCF catalyst with the composition $La_{0.6}Sr_{0.4}Co_{0.8}Fe_{0.2}O_{3-\delta}$. This catalyst is the same composition of the powder that was used to make the supports for the dual-phase membranes. The catalyst is characterized as having a very low BET surface area of 2.85 m^2 g^{-1}. The second catalyst used in this study was a 10 wt % Ni/γ-alumina powder. This particular material has been shown to be effective in reforming reactions such as the one at the center of this work. The nitrogen sorption isotherms are plotted in Figure 4. The isotherm resembles a Type IV isotherm with a hysteresis that appears at a relative pressure of 0.80, indicative of a material having fairly large mesopores. The relatively flat region within the figure suggests that there is formation of a monolayer within the pores of the mesoporous catalyst. The catalyst has a BET surface area of 154.0 m^2 g^{-1}. This value is consistent with previously reported results.[27]

CO_2 permeation through ceramic–carbonate dual-phase membrane with methane sweep

Some work was done on CO_2 permeation through the LSCF–carbonate dual-phase membranes using inert sweeps on the downstream side of the membrane.[21] However, the high-temperature permeation behavior of the membranes using a reducing (methane) sweep has not been studied prior

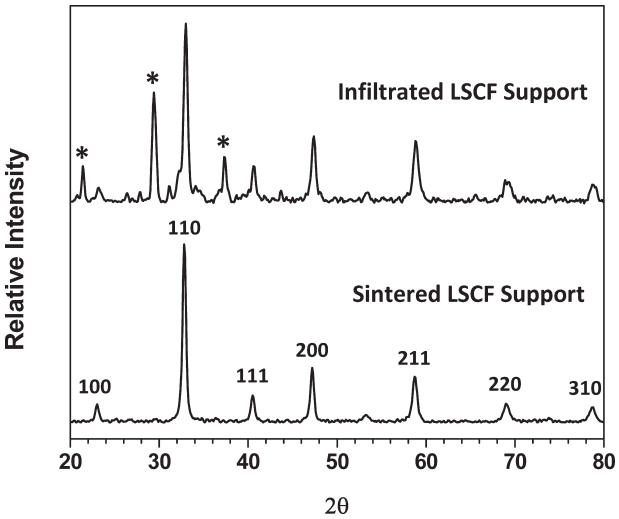

Figure 3. XRD patterns of a sintered LSCF support and carbonate infiltrated membrane (* indicates diffraction peak for carbonate).

The perovskite peaks for the LSCF material are indexed.

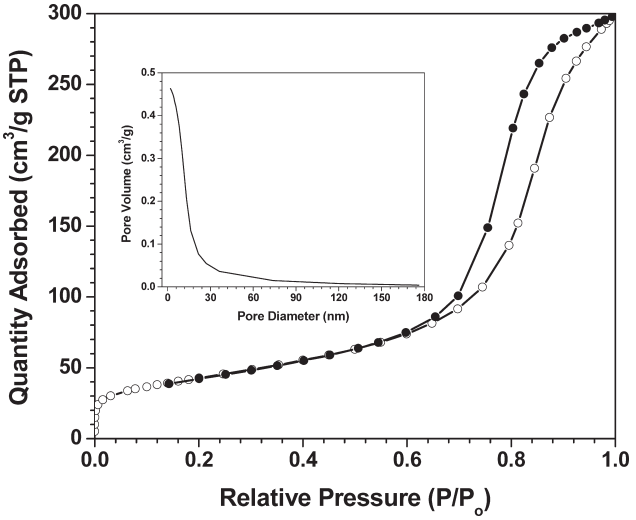

Figure 4. Nitrogen adsorption and desorption isotherms at 77 K for Ni/γ-alumina catalyst.

Absorption ○; Desorption ●. The insets in the figure show the pore-size distribution for the catalyst.

to this work. In order to determine the total flux of CO_2 through the membrane, it was necessary to know both the amount of CO_2 consumed and unconsumed during the dry reforming reaction. Unconsumed CO_2 could be determined directly by GC. The amount of CO_2 consumed by the reaction was dependent on the production rates $\left(Q_{\mathrm{PR}\,(H_2)}\right)$ of H_2 or CO. H_2 and CO are supposed to be produced in a 1:1 ratio during the dry reforming reaction, so the production rate of either species can be used to calculate the total CO_2 flux. In this study, H_2 was chosen due to the greater accuracy in measuring the production rate via the GC. Based on the reaction stoichiometry, the following equation was used to determine the total CO_2 flux that permeated through the membrane in each of the experiments conducted

$$J_{CO_2} = J_{CO_2}(\text{unconsumed}) + \frac{Q_{\mathrm{PR}\,(H_2)}}{2} \tag{1}$$

Measurements were taken from the system that contained no catalyst on the downstream side. This particular arrangement will be referred to as the "blank system." Other systems used in this study involved either the use of the LSCF or Ni/γ-alumina catalysts. When running experiments dealing with changes in methane percentage, the sweep rate (10 mL min^{-1}) and temperature (850°C) were held constant throughout data collection. Similar actions were taken during experiments dealing with changes in sweep rates (methane percentage: 50%; temperature: 850°C) and temperature (methane percentage: 50%; sweep rate: 10 mL min^{-1}). A summary of the variables and constants for each experiment are summarized in Table 1.

In this study, the membranes were found to permeate only CO_2 with measured CO_2/N_2 separation factor larger than 200. Helium gas-tightness data show, theoretically, the membrane should have a much higher CO_2/N_2 selectivity (above 10,000). The lower than expected CO_2/N_2 selectivity measured at high temperature indicates a small amount of leakage through the glass-ceramic seal operated at high temperatures. The dependency of CO_2 permeation upon changing the methane percentage and sweep rate is shown in Figures 5a, b. The figures indicate that neither a change in the concentration of methane in the sweep from 10 to 50% nor a change in the sweep rate from 10 to 50 mL min^{-1} have a significant effect on CO_2 permeation flux. In both figures, the values for CO_2 flux remain at around 0.17 mL min^{-1} cm^{-2} for each adjustment made to either system. The flux measured with the reducing methane sweep compares rather closely to the CO_2 flux obtained from a dual-phase membrane of identical thickness when an inert sweep gas was used (0.16 mL min^{-1} cm^{-2}).[21] As the error in measuring the permeation fluxes was about 8% (which would give error for the permeation flux of ±0.013 mL min^{-1} cm^{-2}), the results show that variation in the methane percentage or sweep gas flow rate by five times caused a change in CO_2 permeation flux within the experimental error.

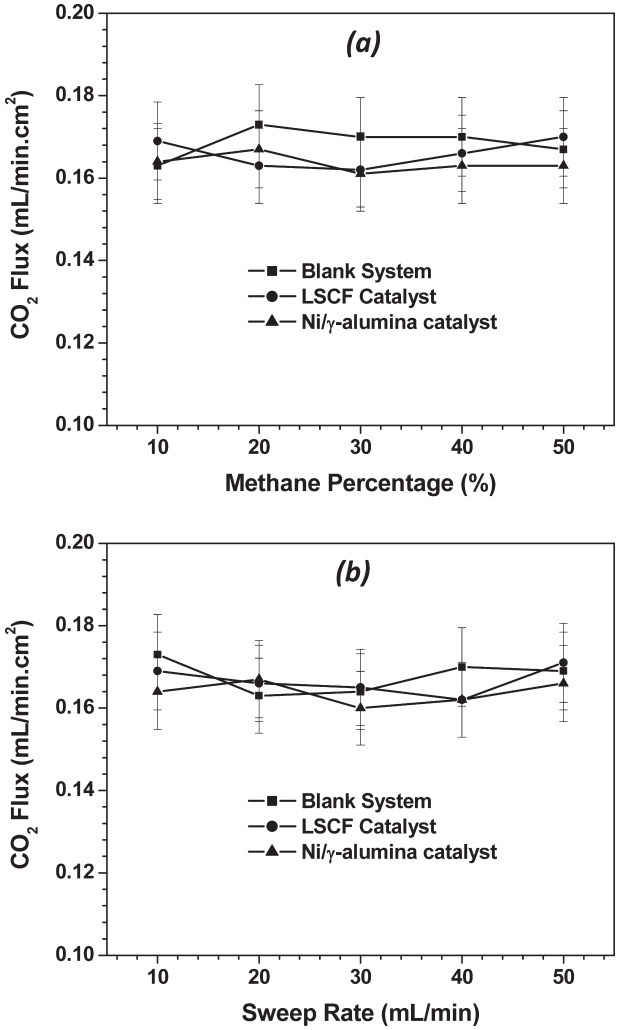

Figure 5. Total CO_2 flux dependency on changing (a) Methane percentage (at sweep flow rate of 10 mL min^{-1}) and (b) Sweep flow rate (at methane percentage of 50%).

Figures 6a, b describe the temperature dependency on CO_2 permeation and the corresponding activation energy, respectively. In Figure 6a, CO_2 flux increases with increasing temperature due to the fact that the ionic conductivity of the support also increases.[28] At the lowest system temperature, the average CO_2 flux with the reducing sweep was 0.061 mL min^{-1} cm^{-2}. The CO_2 flux obtained using an inert sweep gas was 0.068 mL min^{-1} cm^{-2}. At 850°C, the average CO_2

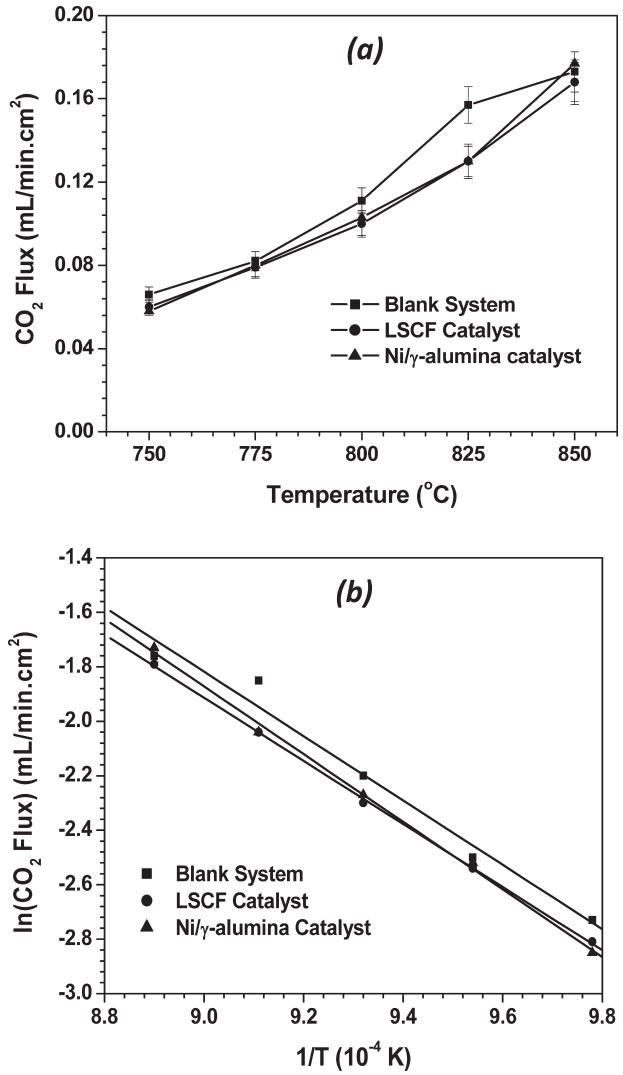

Figure 6. (a) Total CO_2 flux dependency on system temperature; (b) Arrhenius plot of the CO_2 permeation data for the blank system, LSCF, and Ni/γ-alumina catalysts.

flux was 0.17 mL min^{-1} cm^{-2}, similar to 0.16 mL min^{-1} cm^{-2} CO_2 flux measured at the same temperature with a helium sweep.[21] Despite the slight variations, the results obtained in each of the three systems with a reducing sweep are quite comparable to previously reported data obtained with a helium sweep.

Figure 6b shows the Arrhenius plot used to calculate the activation for CO_2 permeation. The activation energies for the three cases were similar, with an average of about 99.3 kJ mol^{-1}, similar to that obtained for the same membrane with the helium sweep.[21] These data show that CO_2 flux has a strong dependency on temperature. Furthermore, the activation energy is similar to that for oxygen ion conductivity of LSCF material. It is known that CO_2 permeation through the ceramic–carbonate dual-phase membrane with the inert sweep gas is controlled by oxygen ionic conduction in the ceramic phase because the oxygen ionic conductivity in the ceramic phase is much lower than the carbonate ionic conductivity in the molten carbonate phase.[29–32] The result obtained here shows that the CO_2 permeation through the dual-phase membrane with methane as the sweep gas is also controlled by the oxygen ionic conduction in the ceramic phase.

The similarity in CO_2 flux values between the reducing and inert gas sweep signifies that the inclusion of methane in the sweep gas does not radically influence CO_2 permeation for the dual-phase LSCF membrane. This is quite different from oxygen permeation through dense LSCF membranes for which oxygen permeation flux with methane sweep is normally several times to one order of magnitude higher than that with just using an inert gas sweep.[33] This difference can be explained by the difference in the reactivity between O_2–CH_4 reaction and CO_2–CH_4 reaction. For oxygen permeation through dense LSCF membrane, oxygen partial pressure in the sweep side (P''_{O_2}) with methane as the sweep gas (e.g., about 10^{-10} atm in methane) is several orders of magnitude lower than that with inert gas as the sweep gas (e.g., about 10^{-3} atm)[33] because of the difference in reactivity between O_2 or CO_2 and CH_4. This is evident that during oxygen permeation experiments with methane as the sweep gas, the oxygen conversion in the sweep side is usually 100%. For dense LSCF membranes, the oxygen permeation flux is related to oxygen partial pressures in the feed and sweep sides (P'_{O_2} and P''_{O_2}) as[33,34]

$$J_{O_2} = \frac{RT\sigma_i^o}{8F^2L}\left(\frac{1}{P''^n_{O_2}} - \frac{1}{P'^n_{O_2}}\right) \quad (2)$$

where σ_i^o is the oxygen ionic conductivity at a reference oxygen partial pressure (normally 1 atm), F is Faraday's constant, L is the membrane thickness, and n is a positive exponent constant that is determined by the dependence of the oxygen ionic conductivity on oxygen partial pressure ($n \sim 8$ for LSCF).[33] As shown by Eq. 2, a difference in the sweep side oxygen partial pressure P''_{O_2} by several orders of magnitude will result in a difference in oxygen permeation flux by several times or up to one order of magnitude. This explains why the oxygen permeation flux through the LSCF membrane with methane as the sweep gas is significantly larger than that with inert gas sweep.

For CO_2 permeation through the dual-phase membrane, the carbon dioxide flux equation is very complex.[30] For semi-quantitative analysis of data, one might use the following simplified equation to correlate CO_2 permeation flux to CO_2 partial pressure in the feed and sweep side, P'_{CO_2} and P''_{CO_2}[22,30]

$$J_{CO_2} = \varphi\frac{RT\sigma_i^o}{4F^2L}\ln\left(\frac{P'_{CO_2}}{P''_{CO_2}}\right) \quad (3)$$

where ϕ is the geometric factor including porosity and tortuosity for the ceramic phase filled with the molten carbonate. Due to the low reactivity between CO_2 and CH_4 as compared to O_2 and CH_4, the CO_2 conversions in the sweep side were typically in the range between 10 and 80% (not like 100% oxygen conversion). Therefore, CO_2 concentration in the sweep side was typically in the range of 0.1–1%. This means that the CO_2 partial pressures in the sweep side without or with methane at different flow rates are in the range of about 0.1–1 $\times$ 10^{-2} atm, or vary by less than one order of magnitude, rather than several orders of magnitude for the oxygen partial pressure in the case of oxygen permeation through dense LSCF membranes (e.g., from 10^{-3} to 10^{-10} atm). Based on Eq. 3, such a small difference in CO_2 partial

pressures would not cause a significant difference in CO_2 permeation flux as compared to oxygen permeation flux through dense LSCF membranes. On the other hand, for a change of CO_2 pressure in the sweep gas by five fold, Eq. 3 predicts a change in CO_2 flux by about 60%. The experimental data obtained here show a change in CO_2 permeation flux less than 8%. It is possibly because Eq. 3 does not adequately describe pressure dependence of CO_2 flux and more work needs to be done to understand the mechanism of CO_2 permeation through the dual-phase membrane with a reducing sweep gas.

Dry reforming of methane for syngas production

Several aspects of the dry reforming reaction were monitored throughout the course of this study. Conversion of both CO_2 and CH_4 was calculated using the products of the dry reforming reaction. To determine the overall conversion of carbon dioxide, the total CO_2 flux calculated from Eq. 1 was required. CO_2 conversion was determined by using the following equation

$$CO_2 \text{ conversion } (\%) = \left(\frac{\frac{1}{2} Q_{PR\,(H_2)}}{J_{CO_2}} \right) \times 100 \tag{4}$$

The amount of methane in the sweep gas was known at all times. The conversion of CH_4 was determined by

$$CH_4 \text{ conversion } (\%) = \left(\frac{\frac{1}{2} Q_{PR\,(H_2)}}{\frac{F_{CH_4}}{A}} \right) \times 100 \tag{5}$$

where F_{CH_4} is the flow rate of methane into the system and A is the area (cm^2) of the dual-phase membrane.

Figures 7a, b show the rate of H_2 production and H_2 to CO ratio when the methane percentage of the sweep gas was changed from 10 to 50%. The sweep rate and temperature of the system were held constant at 10 mL min^{-1} and 850°C, respectively. As shown in Figure 7a, the production rate of H_2 increases in all three of the systems as methane percentage in the sweep increases, reaching maximum H_2 production at a methane concentration of 50%. However, a drastic difference in the production rates can be observed between the Ni/γ-alumina reforming catalyst and the LSCF combustion catalyst or blank system. With the reforming catalyst and a methane concentration of 50%, the production rate of H_2 was 0.27 mL min^{-1} cm^{-2}. In comparison, the rate of production of H_2 is just 0.083 and 0.092 mL min^{-1} cm^{-2} for the blank and combustion catalyst systems under the same experimental conditions. The H_2 to CO ratios in Figure 6b indicate that the production of H_2 and CO was carried out at a 1:1 ratio.

Figures 8a, b reveal the conversion percentages of CO_2 and CH_4, respectively, with different methane percentages in the sweep. From the figures, it is clearly noticeable that conversion of both species increases as methane concentration rises, with one exception, that as methane concentration increases in the Ni/γ-alumina system, conversion of CH_4 drops. For dry reforming of methane on Ni/γ-alumina catalyst, at temperatures above 700°C the reaction rate can be approximated by the following equation[35]

$$r_i = k P_{CH_4}^{a} P_{CO_2}^{b} \tag{6}$$

where i is for either CH_4 or CO_2. The reaction order on CH_4, a, is smaller than 1, and on CO_2, b, larger than 1 at

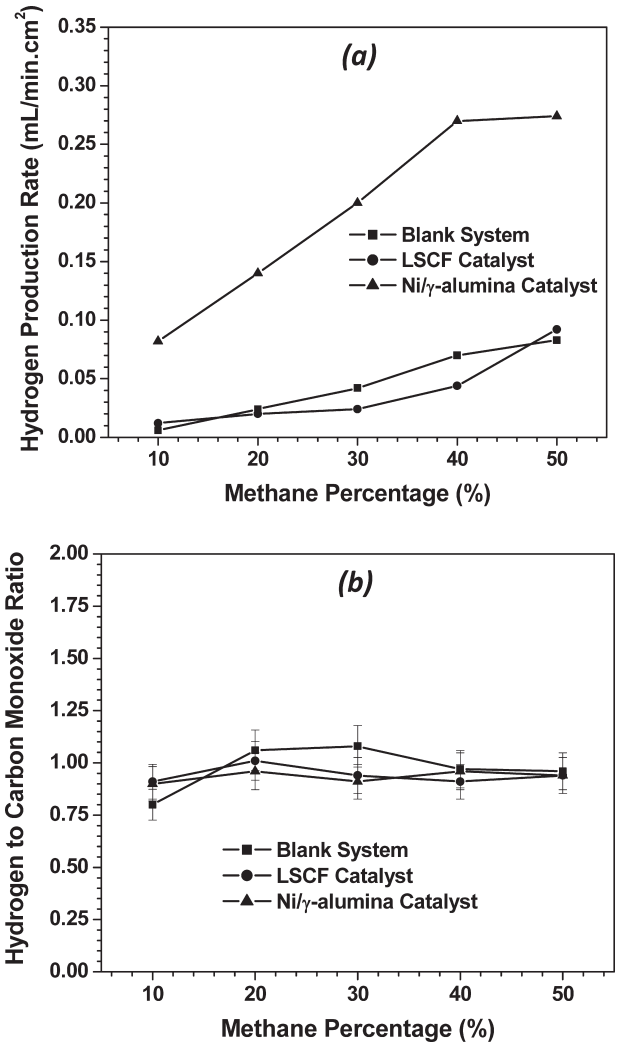

Figure 7. Effects of methane percentage in the sweep gas at flow rate of 10 mL min^{-1} at 850°C on (a) hydrogen production rate and (b) ratio of hydrogen to carbon monoxide formation rates.

temperatures above 700°C.[35] As the CO_2 permeation flux is essentially constant over different methane concentrations, the feed concentration of CO_2 in the sweep (reaction) side can be considered constant. Integration of Eq. 6 for the reactor (assuming fixed-bed) would give a CH_4 conversion that decreases with increasing CH_4 feed concentration for $a<1$. The CO_2 conversion, from the integration result, would increase with increasing CH_4 feed concentration as long as $a>0$ because in this reactor the CO_2 feed concentration (determined by CO_2 permeation) essentially does not change as CH_4 feed concentration increases. Finally, the CO_2 conversions are higher than CH_4 conversion because CO_2 fluxes through the membrane are on the order of 10^{-1} mL min^{-1} cm^{-2}, much lower than area normalized methane feed rates on the order of 10^{1} mL min^{-1} cm^{-2}.

The highest conversions of CO_2 were achieved when methane concentration was 50%. Carbon dioxide conversion with the LSCF combustion catalyst and blank system are low, never breaching 32%. The probability that CO_2 and CH_4 will interact on the surface of membrane or within the catalyst bed increases at higher methane concentration. However, the low

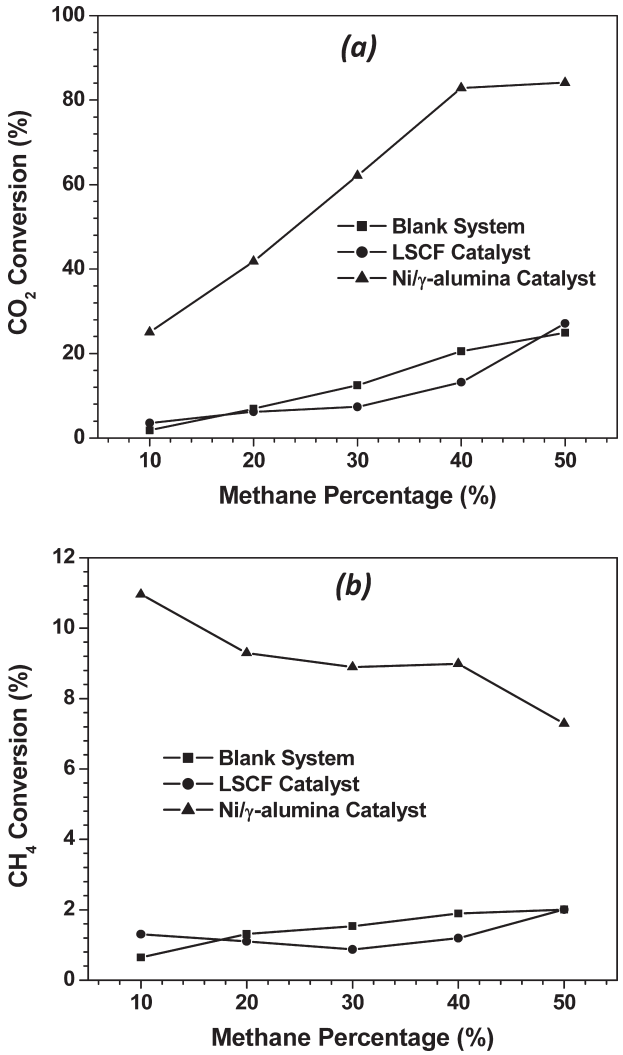

Figure 8. CO_2 conversion (a) and CH_4 conversion (b) at different methane percentage in the sweep gas (at 850°C and sweep flow rate of 10 mL min^{-1}).

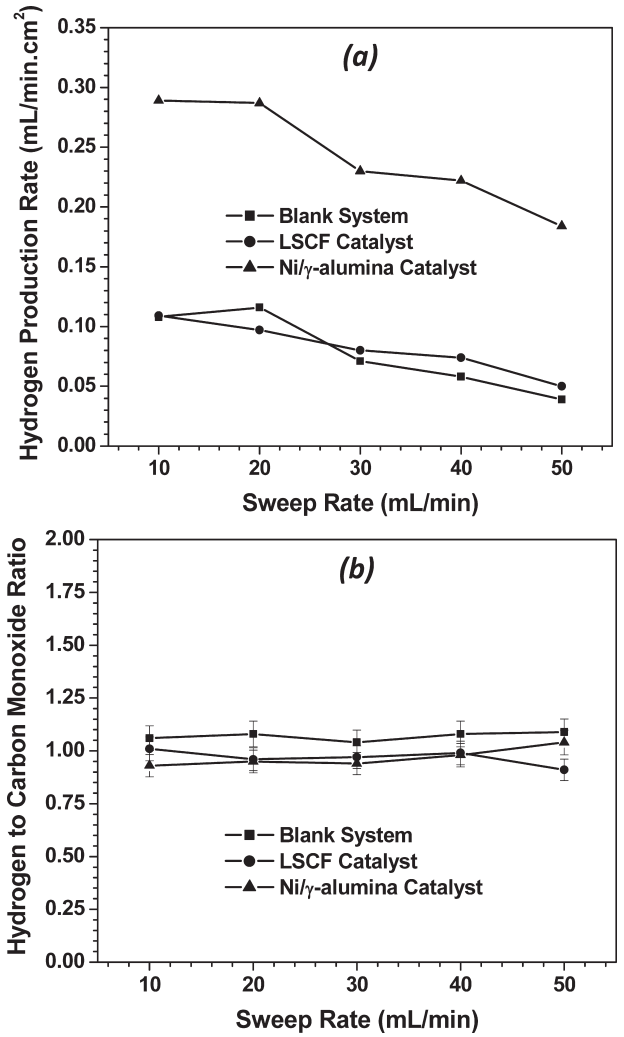

Figure 9. Effects of sweep flow rate on (a) hydrogen production rate and (b) ratio of hydrogen to carbon monoxide formation rates (at 850°C and methane percentage of 50%).

surface area of the LSCF catalyst provides no obvious improvement in comparison to the blank system. A catalyst with much higher area and activity would be more suitable for this type of system which was confirmed by the addition of the Ni/γ-alumina catalyst.

Figures 9a, b show the rate of H_2 production when sweep flow rate on the downstream side of the dual-phase membrane was increased from 10 to 50 mL min^{-1} for the blank system, and the systems with LSCF and Ni- alumina catalysts. For this particular set of experiments, the methane concentration in the sweep and temperature of the system were held constant at 50% and 850°C, respectively. In Figure 9a, the production of syngas is maximized in the Ni/γ-alumina catalyst system at a sweep rate of 10 mL min^{-1}. Here, the H_2 production rate is 0.29 mL min^{-1} cm^{-2}. Conversely, for a sweep rate of 50 mL min^{-1}, the production rate drops by about 40% to 0.18 mL min^{-1} cm^{-2}. Even at low sweep rates, the production of H_2 in the LSCF catalyst or blank system never reaches a rate greater than 0.11 mL min^{-1} cm^{-2}. Figure 9b shows the H_2:CO ratio achieved with increasing sweep flow rate on the downstream side of the membrane. As was the case in Figure 7b, the general trend here indicates that the ratio of products is about 1, regardless of whether or not the sweep rate is low or high.

Figure 10a shows that as sweep flow rate increases, CO_2 conversion decreases for each of the systems in this study. The CO_2 conversions achieved at a sweep rate of 10 mL min^{-1} for the blank system, LSCF and Ni/γ-alumina catalysts were 31.2, 31.9, and 88.3%, respectively. In comparison, for an increase in sweep rate to 50 mL min^{-1}, the conversions decreased to 11.4, 14.7, and 55.4%. The same general trend for methane conversion is depicted in Figure 10b. However, the conversion drops to less than 0.60% when the sweep rate is increased by a factor of 5. While the values are for the Ni/γ-alumina system are low, the conversion rates are even lower in the LSCF catalyst and blank systems at roughly 0.15%. The decrease in syngas production with increase in sweep rate can be ascribed to the fact that the reactants (CH_4 and CO_2) are swept away from the surface of the membrane or from within the catalyst bed at a faster rate. The increase in sweep rate leads to lower residence time. The low residence time does not allow for the dry reforming reaction to take place.[36] Again, the conversion of CO_2 and CH_4 to syngas is very low as a result of the very

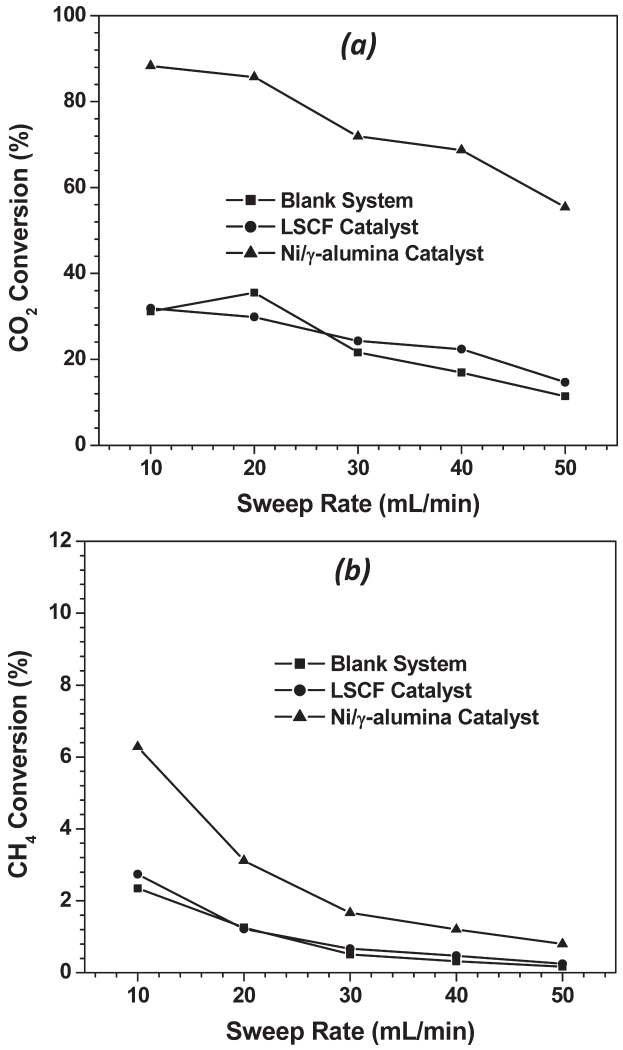

Figure 10. CO_2 conversion (a) and CH_4 conversion (b) at various sweep flow rate (at 850°C and methane percentage of 50%).

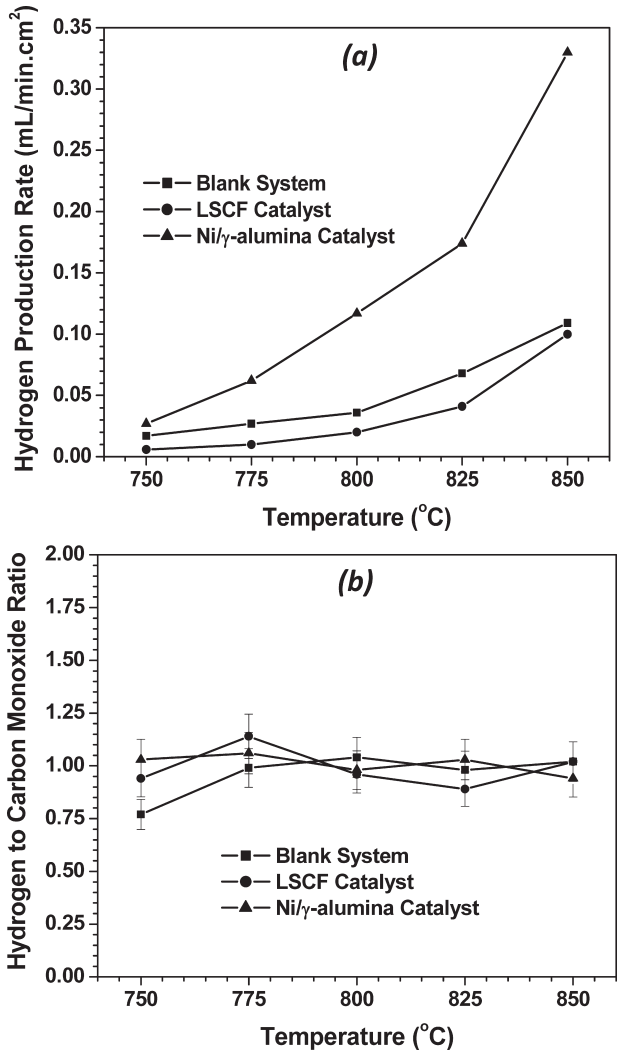

Figure 11. Effects of temperature on (a) hydrogen production rate and (b) ratio of hydrogen to carbon monoxide formation rates.

low surface areas for reaction for the LSCF catalyst and blank systems. The use of the reforming catalyst was the only method by which syngas was produced in reasonable amounts.

Figures 11a, b show the rate of H_2 production and H_2 to CO ratio at different temperatures in 750–850°C. For this portion of the study, the methane percentage in the sweep and the sweep rate were held constant at 50% and 10 mL min^{-1}, respectively. As Figure 11a clearly shows, the production of hydrogen is greatly enhanced at high temperatures. Furthermore, the addition of the Ni/γ-alumina catalyst in conjunction with higher system temperature further increases the production of H_2. At 850°C, the production rate of H_2 is 0.10 and 0.11 mL min^{-1} cm^{-2} for the LSCF catalyst and blank systems. For the same conditions in the Ni/γ-alumina system, the production of H_2 is more than triple at 0.33 mL min^{-1} cm^{-2}. However, the profound effect of the Ni/γ-alumina catalyst is less pronounced at lower temperatures. The H_2 to CO formation rate ratio for all the three reactor systems is close to 1, indicating negligible amount of side reactions. Only for the blank system at 750°C, the H_2 to CO formation rate is lower than 1 (about 0.8), indicating that reverse water gas shift reaction that consumes H_2 might be important. The H_2 to CO ratio for the blank system approaches 1 as dry reforming reaction becomes dominant at higher temperature.

The conversion of CO_2 and CH_4 decreases as temperature decreases, as shown in Figures 12a, b. Similar to the other experiments performed in this work, the maximum CO_2 and CH_4 conversions were experienced when using the dual-phase membrane in conjunction with the Ni/γ-alumina catalyst. At 850°C, the conversions in this case were 93.3 and 7.2%, respectively. Drastic drops in the conversions of both gases occur at 750°C, decreasing to 23.1% for CO_2 and 0.58% for CH_4. Similar characteristics were observed for the LSCF catalyst and blank systems. Despite the presence of the LSCF combustion catalyst, little to no improvement was achieved in comparison to the results obtained for the blank system.

Comparison of the three membrane reactor systems and membrane stability

The nine experiments conducted in this study were all designed to share one point in common for comparison sake. These points represent the perceived optimum (i.e., favorable) conditions for syngas production, which are high methane

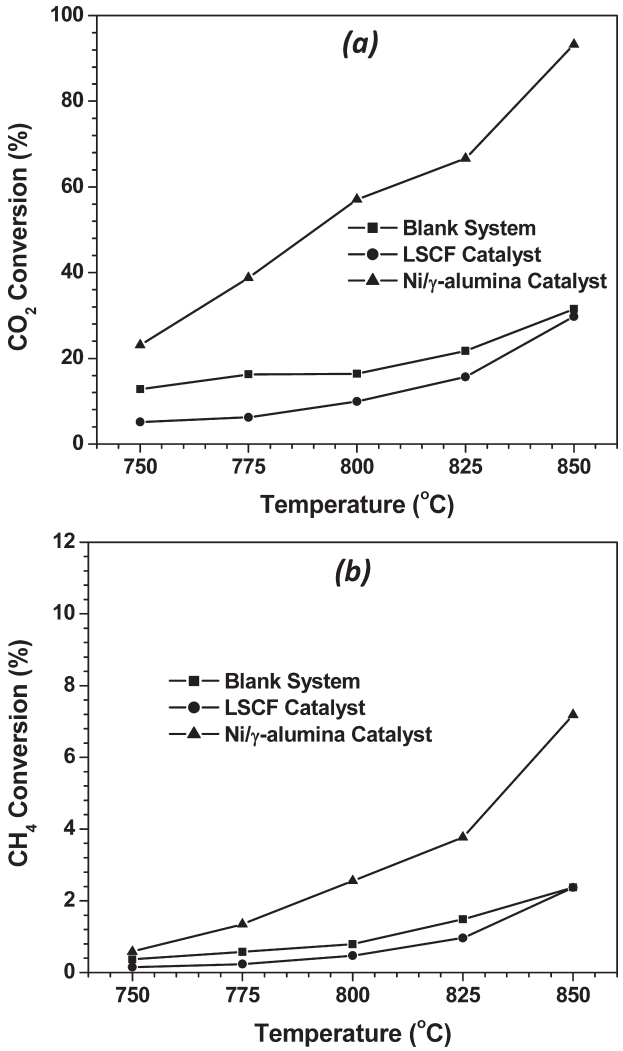

Figure 12. Effects of temperature on (a) CO_2 conversion and (b) CH_4 conversion (at methane percentage of 50% and sweep rate of 10 mL min^{-1}).

percentage (50%), low sweep rate (10 mL min^{-1}) and high temperature (850°C). The three points in common have been averaged and summarized in the Table 2. From Table 2, it can be inferred that the addition of either catalyst had negligible effect on CO_2 permeation through the membrane. In terms of syngas production, the addition of the LSCF catalyst did nothing to improve performance. While it was believed that the blank system would provide the poorest results, it was unexpected to see the blank system and LSCF catalyst perform so similarly. The lack of improvement observed for the use of the LSCF catalyst in this study is ascribed to the fact that the LSCF catalyst does not have a sufficiently high surface area. Furthermore, perovskite-type catalysts like LSCF are more suitable for combustion reactions rather than reforming reactions.[37] In addition, it took 1.0 g of catalyst to create a bed height of 3 mm for the LSCF catalyst. The more densely packed bed, and hence lower void volumes, could have limited the flow of gases within the bed and also contributed to the low reactivity within the system. For these reasons, the results gathered from using the LSCF catalyst are no better than those obtained when using just the surface of the LSCF–carbonate membrane to enhance the reaction.

The use of the mesoporous Ni/γ-alumina catalyst led to high conversions in each of the cases involved in this work. Pompeo et al.[37] and Lui et al.[38] reported similar results for conversions of CO_2 via dry reforming at elevated temperatures. Haag et al.[39] also demonstrated that the calculated equilibrium conversion of CO_2 in dry reforming reactions is greater than 90% at temperatures above 850°C. At that temperature, the conversion of CO_2 was near or above 90% for each case in this work. On the other hand, Haag et al. also demonstrated that CO_2 conversion at 750°C was in the 80% range. In this work, CO_2 conversion at that temperature was only 38% at 750°C with the Ni/γ-alumina catalyst. The lack of conversion at the lower system temperature can possibly be attributed to less than optimal conditions (tube placement with regards to the catalyst beds) within the permeation setup.

It should be noted that the loading of Ni was kept low at 10% to limit deactivation of the catalyst. Ni-based catalysts with a loading above 10 wt % metal have been shown to be prone to deactivation as a result of carbon deposition. Arena et al.[40] indicated that the presence of these alkali earth metals within catalysts could improve the catalytic stability and activity of various materials. The molten carbonate used to infiltrate the membrane contains lithium, sodium, and potassium—all alkali earth metals, which, if get into the catalyst, can help stabilize the catalysts.

XRD analysis performed on both the Ni/γ-alumina and LSCF catalysts before and after the reactions showed no discernable change in the patterns. Overall carbon balances in and out of the systems showed no noticeable accumulation within the system. This carbon balance result plus the absence of carbon diffraction peaks on the tested catalysts indicate negligible amount of coke formed during the reaction. Furthermore, the approximate unity ratio of H_2 to CO formation rates measured in this work suggest no side reactions such as the Boudouard, methane cracking, or reserve water gas shift reaction during the dry reforming reaction in the membrane reactor.

XRD results obtained from analysis of the LSCF–carbonate dual-phase membrane in the dry reforming experiment with the Ni/γ-alumina reforming catalyst are shown in Figure 13 in order to compare the characteristics of untarnished membranes. For the most part, it appears that the perovskite structure of the support remains relatively unchanged. It is known that LSCF is unstable in CO_2 atmospheres at high temperature, with possible reactions to form $SrCO_3$ and metal oxides of La, Co, and Fe.[41] As the experiments were conducted only for a few days, it is possible that the reaction time was not sufficiently long enough to observe the reaction of LSCF with CO_2 on the membrane surface. The other

Table 2. Summary of Data Obtained from Figures 4–11

Catalyst	CO_2 Flux (mL min^{-1} cm^{-2})	H_2 Production Rate (mL min^{-1} cm^{-2})	H_2:CO Ratio	CO_2 Conversion (%)	CH_4 Conversion (%)
Blank	0.17	0.10	0.92	29.2	2.2
LSCF	0.17	0.10	0.99	29.5	2.4
Ni/γ-alumina	0.17	0.30	1.01	88.5	8.1

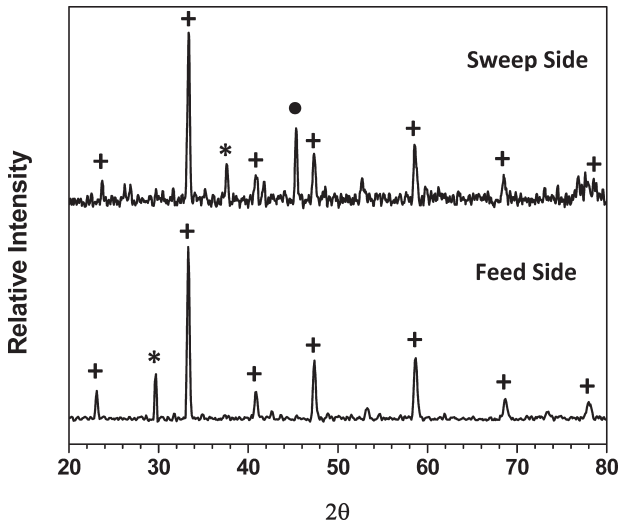

Figure 13. XRD patterns of the feed (CO_2) and sweep (CH_4) side of a LSCF–carbonate dual-phase membrane after the dry reforming reaction using the Ni/γ-alumina catalyst (+, *, and ● indicate diffraction peaks for perovskite, carbonate, and unknown structures, respectively).

possibility is that the presence of the metal carbonate phase retards the reaction of LSCF with gas-phase CO_2.

However, Figure 13 shows that there are noticeable differences in the appearance, or lack thereof, of the molten carbonate peaks between the two sides of the membrane disk after the experiments. For the feed side, the dominant peak indicating the presence of molten carbonate at 29.4° is less intense than that of a freshly infiltrated membrane. Furthermore, the minor peak indicating the presence of molten carbonate at 37.3° is not visible in the pattern. The results for the sweep side XRD pattern of the membrane are vice versa. Although there was a peak at 29.4° for the feed side, the peak is absent on the sweep side pattern. However, unlike the feed side, the molten carbonate peak at 37.3° is present. Although these changes are somewhat peculiar and not completely understood, the results are likely linked to the decomposition partial pressure of molten carbonate mixture used in this work.

The feed side is consistently at a feed CO_2 at a partial pressure of 0.25 atm. This is well above the decomposition partial pressure of the molten carbonate within the membrane. However, the CO_2 partial pressure on the sweep side is below the decomposition partial pressure. Furthermore, there is the inclusion of an additional peak at approximately 46.0°. This peak may correspond to a metal oxide formed due to decomposition reaction of molten carbonate near the sweep side surface at the initial period of reaction after methane was introduced to the sweep side. It was found that for a short period of time (less than 1 h), there was a small amount of measured CO_2 on the downstream side without CO_2 in the feed. This indicates that decomposition was the source of CO_2 in the first hour. However, after a period of more than 1 h, this was no longer observed. Thus, it is possible that at the startup of the dry-reforming reaction process in the membrane reactor, before a steady-state CO_2 concentration profile was established across the membrane, some of the molten carbonate on the sweep side surface decomposed. Once the steady-state CO_2 concentration profile in the membrane was established, CO_2 permeated from the upstream surface would ensure sufficiently high CO_2 chemical potential on the sweep side surface of the membrane. This would prevent carbonate from further decomposition.

Due to sealing issues, long-term performance tests could not be attempted. However, if long-term experiments are to be carried out in the future, catalysts capable of withstanding the harsh conditions present during the dry reforming reaction for a long period of time would likely be necessary. Pompeo et al.[2] described the use of a α-alumina supported Ni catalyst that was modified with zirconia (ZrO_2) to improve long-term stability and activity. Cerium IV Oxide could also be used, as it has been shown to increase the effectiveness of Ni–alumina-based catalysts.[42]

It should be pointed out that the feed stream in these experiments merely mimicked flue gas, using only CO_2 and N_2. Real flue gas contains O_2, H_2O, and other trace impurities in addition to CO_2 and N_2. As the dual-phase membrane with an oxygen ionic conducting (not mixed conducting) ceramic phase is perm-selective only to CO_2, not the other gases,[31] the presence of the additional gases in the flue gas should not affect the general trends of the results for dry reforming reaction of methane and CO_2 permeation reported here. However, the effects of these additional gases, such as H_2O vapor or trace impurities, on membrane stability and CO_2 permeation rates are unknown and need to be studied in the future.

Conclusions

This work demonstrated successful coupling of separation of carbon oxide from carbon dioxide–nitrogen mixture with dry reforming of methane to produce synthesis gas by a ceramic–carbonate dual-phase membrane at high temperatures (750–850°C). Under the experimental conditions, CO_2 permeation flow rate matches the dry-reforming reaction rate and the CO_2 conversion as high as 88% can be achieved in the dual-phase membrane reactor packed with an active dry reforming catalyst. The syngas produced has a H_2:CO ratio approximately equal to 1 under various reaction conditions. The conversion of CO_2 and CH_4 to syngas increases in the order of blank system < LSCF combustion catalyst < Ni/γ-alumina reforming catalyst due to the increase in the catalytic activity. However, the CO_2 permeation flux remains essentially constant with the dry reforming reaction on different catalysts under various methane concentrations or sweep gas flow rates. The average CO_2 permeation flux was about 0.17 mL cm^{-2} min^{-1} at 850°C with an activation energy for permeation of about 99.3 kJ mol^{-1}, similar to that for oxygen ion conduction in the bulk ceramic phase used in the membrane. There are essentially no side reactions observed for the dry reforming of methane in the membrane reactor. The work shows promise of this new membrane reactor for dry reforming of methane, but it calls for more studies to understand the effects of downstream conditions on CO_2 permeation and performance and stability of the membrane with a feed that resembles real flue gas.

Acknowledgments

The authors acknowledge the support of Department of Energy (DE-FE000470) and National Science Foundation (CBET-0828146) on the study. MA would like to acknowledge the support of Dean's graduate fellowship during his graduate study at ASU. The authors would also like to

acknowledge Tyler Norton and Shriya Seshadri for their assistance on this project. We gratefully acknowledge the support and use of the facilities in the LeRoy Eyring Center for Solid State Sciences (LE-CSSS) at Arizona State University.

Literature Cited

1. Prabhu AK, Oyama ST. Highly hydrogen selective ceramic membranes: application to the transformation of greenhouse gases. *J Membr Sci*. 2000;176:233–248.
2. Pompeo F, Nichio NN, Ferretti OA, Resasco D. Study of Ni catalysts on different supports to obtain synthesis gas. *Int J Hydrogen Energy*. 2005;30:1399–1405.
3. Tong J, Yang W, Cai R, Zhu B, Lin L. Novel and ideal zirconium-based dense membrane reactors for partial oxidation of methane to syngas. *Catal Lett*. 2002;78:129–137.
4. Bouwmeester HJM. Dense ceramic membranes for methane conversion. *Catal Today*. 2003;82:141–150.
5. Shao Z, Xiong G, Dong H, Yang W, Lin L. Synthesis, oxygen permeation study and membrane performance of a $Ba_{0.5}Sr_{0.5}Co_{0.8}Fe_{0.2}O_{3-\delta}$ oxygen-permeable dense ceramic reactor for partial oxidation of methane to syngas. *Sep Purif Technol*. 2001;25:97–116.
6. Balachandran U, Dusek JT, Maiya PS, Ma B, Mieville RL, Kleefisch MS, Udovich CA. Ceramic membrane reactor for converting methane to syngas. *Catal Today*. 1997;36:265–272.
7. Dong H, Shao Z, Xiong G, Tong J, Sheng S, Yang W. Investigation on POM reaction in a new perovskite membrane reactor. *Catal Today*. 2001;67:3–13.
8. Luo H, Wei Y, Jiang H, Yuan W, Lv Y, Caro J, Wang H. Performance of a ceramic membrane reactor with high oxygen flux Ta-containing perovskite for the partial oxidation of methane to syngas. *J Membr Sci*. 2010;350:154–160.
9. Wang H, Cong Y, Yang W., Investigation on the partial oxidation of methane to syngas in a tubular $Ba_{0.5}Sr_{0.5}Co_{0.8}Fe_{0.2}O_{3-\delta}$ membrane reactor. *Catal Today*. 2003;82:157–166.
10. Ikeguchi M, Mimura T, Sekine Y, Kikuchi E, Matsukata M. Reaction and oxygen permeation studies in $Sm_{0.4}Ba_{0.6}Fe_{0.8}Co_{0.2}O_{3-\delta}$ membrane reactor for partial oxidation of methane to syngas. *Appl Catal A- Gen*. 2005;290:212–220.
11. Balachandran U, Dusek JT, Mieville RL, Poeppel RB, Kleefisch MS, Pei S, Kobylinski TP, Udovich CA, Bose AC. Dense ceramic membranes for partial oxidation of methane to syngas. *Appl Catal. A-Gen*. 1995;133:19–29.
12. Wang S, Lu GQ, Miller GJ. Carbon dioxide reforming of methane to produce synthesis gas over metal-supported catalysts: state of the art, *Energy Fuel*. 1996;10:896–904.
13. Rostrup-Nielsen JR. Aspects of CO_2-reforming of methane. *Stud Surf Sci Catal*. 1994;81:25–41.
14. Lemoniodu AA, Goula MA, Vasalos IA. Carbon dioxide reforming of methane over 5 wt.% nickel calcium aluminate catalysts – effect of preparation method. *Catal Today*. 1998;46:175–183.
15. Hou Z, Yokota O, Tanaka T, Yashima T. Characterization of Ca-promoted Ni/α-Alumina catalyst for CH_4 reforming with CO_2. *Appl Catal A: Gen*. 2003;253:381–387.
16. Juan-Juan J, Román-Martínez MC, Illán-Gómez MJ. Catalytic activity and characterization of Ni/Alumina and NiK/Alumina catalysts for CO_2 methane reforming. *Appl Catal A: Gen*. 2004;264:169–174.
17. Edwards JH, Maitra AM. The chemistry of methane reforming with carbon dioxide and its current and potential applications. *Fuel Process Technol*. 1995;42:269–289.
18. Prabhu AK, Radhakrishnan R, Oyama ST. Supported nickel catalysts for carbon dioxide reforming of methane in plug flow membrane reactors. *Appl Catal A: Gen*. 1999;183:241–252.
19. Gallucci F, Toshi S, Basile A. Pd-Ag tubular membrane reactors for methane dry reforming: A reactive method for CO_2 consumption and H_2 production. *J Membr Sci*. 2008;317:96–105.
20. Bosko ML, Munera JF, Lombardo EA, Cornaglia LM. Dry reforming of methane in membrane reactors using Pd and Pd-Ag composite membranes on a NaA modified porous stainless steel support. *J Membr Sci*. 2010;364:17–26.
21. Anderson M, Lin YS. Carbonate-ceramic dual-phase membrane for carbon dioxide separation. *J Membr Sci*. 2010;357:122–129.
22. Chung S, Park J, Li D, Ida J-I, Kumakiri I, Lin YS. Dual-phase metal-carbonate membrane for high-temperature carbon dioxide separation. *Ind Eng Chem Res*. 2005;44:7999–8006.
23. Qi X, Akin FT, Lin YS. Ceramic–glass composite high temperature seals for dense ionic-conducting ceramic membranes. *J Membr Sci*. 2001;193:185–193.
24. Wang S, Katsuki M, Dokiya M, Hashimoto T. High temperature properties of $La_{0.6}Sr_{0.4}Co_{0.8}Fe_{0.2}O_{3-\delta}$ phase structure and electrical conductivity. *Solid State Ionics* 2003;159:71–78.
25. Choudhary VR, Uphade BS, Belhekar AA. Oxidative conversion of methane to syngas over $LaNiO_3$ perovskite with or without simultaneous steam and CO_2 reforming reactions: influence of partial substitution of La and Ni. *J Catal*. 1996;25:312–318.
26. Choudhary VR, Uphade BS, Pataskar SG. Low temperature complete combustion of methane over Ag-doped $LaFeO_3$ and $LaFe_{0.5}Co_{0.5}O_3$ perovskite oxide catalysts. *Fuel*. 1999;78:919–921.
27. Goncalves G, Lenzi MK, Santos OAA, Jorge LMM. Preparation and characterization of nickel based catalysts on silica, alumina and titania obtained via the sol-gel method. *J Non-Cryst Solids* 2006;352:3697–3704.
28. Teraoka Y, Zhang H, Okamoto K, Yamazoe N. Mixed ionic-electronic conductivity of $La_{1-x}Sr_xCo_{1-y}Fe_yO_{3-\delta}$ perovskite-type oxides. *Mater Res Bull*. 1998;23:51–58.
29. Wade JL, Lee C, West AC, Lackner KS. Composite electrolyte membranes for high temperature CO_2 separation, *J Membr Sci*. 2011;369:20–29.
30. Rui Z, Anderson M, Lin YS, Li Y. Modeling and analysis of carbon dioxide permeation through ceramic-carbonate dual phase membranes. *J Membr Sci*. 2009;345:110–118.
31. Rui, Z, Anderson M., Li Y, Lin YS. Ionic conducting ceramic and carbonate dual phase membranes for carbon dioxide separation. *J Membr Sci*. 2012;417-418:174–182.
32. Zhang LL, Xu NS, Li X, Wang SW, Huang K, Harris WH, Chiu WKS. High CO2 permeation flux enabled by highly interconnected three-dimensional ionic channels in selective CO2 separation membranes. *Energy Environ Sci*. 2012;5:8310–8317.
33. Akin FT, Lin YS. Oxygen permeation through oxygen ionic or mixed-conducting ceramic membranes with chemical reactions. *J Membr Sci*. 2004;231:133–146.
34. Norton TT, Lin YS. Transient oxygen permeation and surface catalytic properties of lanthanum cobaltite membrane under oxygen-methane gradient. *Ind Eng Chem Res*. 2012;51:12917–12925.
35. Wang S, Lu G.Q. A comparative study on carbon dioxide reforming of methane over Ni/γ-Al_2O_3 Catalysts. *Ind Eng Chem Res*. 1999;38:2615–2625.
36. Zawadzki M, Trawczyński J. Synthesis, characterization and catalytic performance of LSCF perovskite for VOC combustion. *Catal Today*. 2011;176:449–452.
37. Pompeo F, Nichio NN, Souza MMVM, Cesar DV, Ferretti OA, Schmal M. Study of Ni and Pt catalysts supported on α-Alumina and ZrO_2 applied in methane reforming with CO_2. *Appl Catal A. Gen*. 2007;316:175–183.
38. Lui BS, Gao LZ, Au CT. Preparation, characterization and application of catalytic NaA membrane for CH_4/CO_2 reforming to syngas. *Appl Catal A: Gen*. 2002;235:193–206.
39. Haag S, Burgard M, Ernst B. Beneficial effects of the use of a nickel membrane reactor for the dry reforming of methane: comparison with thermodynamic equilibrium. *J Catal*. 2007;252:190–204.
40. Arena F, Frusteri F, Parmaliana A. Alkali promotion of Ni/MgO catalysts. *Appl Catal A: Gen*. 1996;145:127–140.
41. Yang Q, Lin YS. Kinetics of carbon dioxide sorption on perovskite type metal oxides. *Ind Eng Chem Res*. 2006;45:6302–6310.
42. Laosiripojana N, Sutthisripok W, Assabumrungrat S. Synthesis gas production from dry reforming of methane over CeO_2 doped Ni/Alumina: influence of doping ceria on the resistance toward carbon formation. *Chem Eng J*. 2005;112:13–22.

Manuscript received Jun. 1, 2012, and revision received Dec. 3, 2012.